

Chapter 7

Pruning in billiards

We now give a pruning front description of the admissible orbits in all billiard introduced in chapter 6. The pruning fronts are then approximated by converging sequences of approximate fronts which give finite Markov diagram description of the symbol strings of the admissible orbits.

7.1 Singular points

In the smooth two-dimensional folding maps such as the Hénon map, the pruning front is a symbolic representation of the primary turning points of the unstable manifold. Also in the piecewise linear Lozi map the kneading sequences from all primary (non-smooth) turning points mapped into the well ordered symbol plane define the pruning front. The Lozi map manifolds, figure 5.20, gives the most useful image in motivating our approach to determining pruning fronts in the billiard systems. Pictures of the manifolds of orbits in the 3 disk system and the stadium billiard are shown in figures 7.1 and 6.12. The manifolds have a structure similar to the Lozi map manifolds, figure 5.20, except that in a close billiard both manifolds are dense in the phase space. The manifolds are smooth lines changing direction at a singular points which we for the Lozi map called the turning points. The manifolds of the wedge/two ball problem, figure 6.10, and the overlapping disks are slightly different because the manifolds end at a singular point, but then continue somewhere else in the phase space instead of just change direction. To understand why these manifolds are discontinuous, we investigate closer the singularities in the different billiards.

For a dispersive billiard the point corresponding to the turning point of a $2-d$ map is the orbit touching the wall tangentially. Figure 7.2 shows how a line is folded at a dispersing wall and the point moving tangential to the wall is the turning point

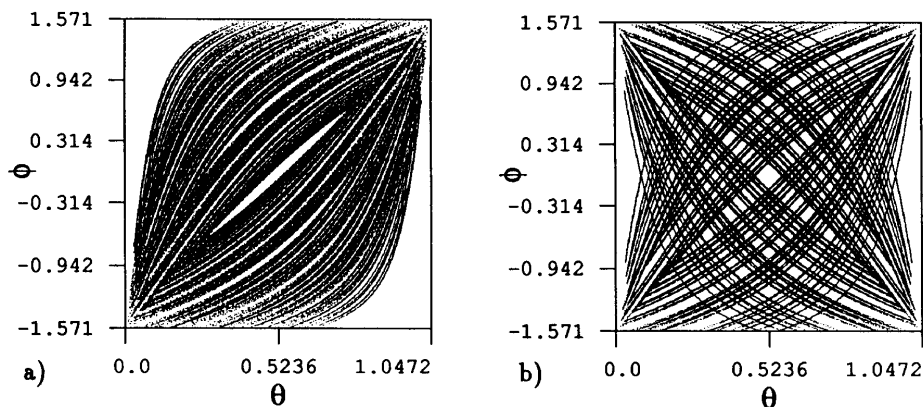


Figure 7.1: A part of the manifold of the orbit $s: \overline{123}$ in the touching 3 disk system, $r = 2$. a) The unstable manifold. b) The stable and unstable manifold.

of the folding. This orbit is usually called the singular orbit [181]. This grazing orbit in the dispersing billiard plays the same role in this system as the critical point in a unimodal map and the pruning front can be constructed by finding the symbol string (kneading sequence) of all orbits grazing the wall of the billiard domain.

The stadium billiard [32] has a singular point where a semi-circle joins a straight line. Figure 7.3 shows how a line of phase space points is folded when reflected in the neighborhood of a singular point. The picture is similar to the dispersive billiard; the curve after the folding is continuous with one sharp turning point. The turning point is the singular orbit bouncing off the singular point on the wall. At this point the wall is continuous and has a continuous first derivative but the second derivative is discontinuous. This gives the sharp folding of the neighborhood of the orbit through the singular point, acting as the turning point. The symbol strings for all orbits that bounce with different angles through this singular point yield a pruning front in a well-ordered symbol plane.

In the wedge billiard, as well as in the overlapping dispersive billiards, the folding of curves is qualitatively different than in the stadium and the non-overlapping dispersive billiards because a curve breaks up into two disconnected parts at the singular orbit. In other billiards the limit orbits from each side of the singular orbit converge to the same orbit, but this is not true in general, see figure 7.4. This is the simplest way a curve can break up, but if the incoming angle or the angles of the walls close to the corner are different, the limiting orbits to the singular point may bounce more than once close to the corner. In the integrable $\theta = 45^\circ$ limit for the wedge billiard, the two limit orbits to the tip point are identical to each other for all incoming angles, and the same is of course true for $\theta = 90^\circ$. Smilansky [185] has

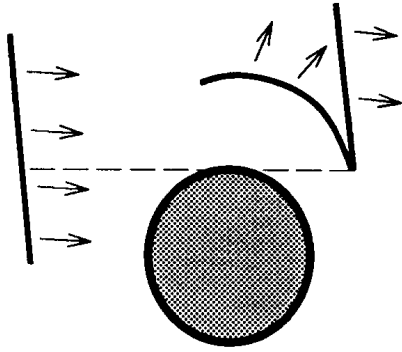


Figure 7.2: Folding of a line in the configuration space when bouncing off a dispersing wall.

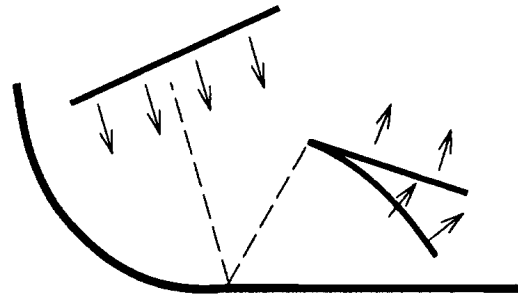


Figure 7.3: Folding of a line in the configuration space when bouncing off the stadium close to the singular point.

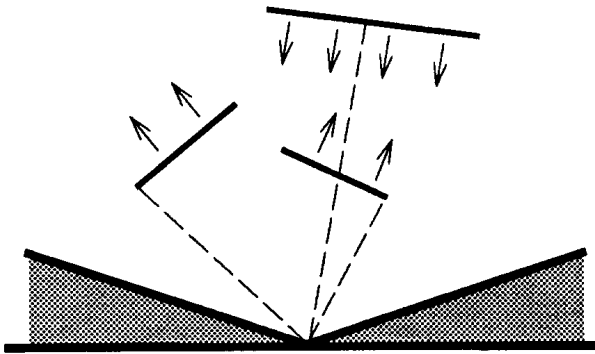


Figure 7.4: The breakup of a line in the configuration space when bouncing off a corner in the wedge billiard, or an overlapping disk system.

observed that for $\theta = 60^\circ$ many orbits return out in the same direction independent of whether they bounce to the right or to the left of the tip point. There may be other exceptions of this kind, but in general the folds are discontinuous as, for example, the manifold in figure 6.10. This makes the problem less like the Lozi map, and more like a two-dimensional version of a Bernoulli shift.

Discontinuity of folding does not lead to any problems in determining the pruning front. The pruning front is given by the symbolic strings of the two limits to the singular orbit, bouncing close to the corner with varying incidence angles. We let the orbits bounce off one of the two walls, and scan all outgoing angles (in the wedge billiard from $-\theta$ to θ); the symbol strings for each angle yields a point on the pruning front. If the folding had been continuous, we would only have scanned the angles between 0 and θ , so the consequence of the discontinuity is less symmetry in

the pruning front.

Similarly, in a dispersing billiard that has a corner with a finite angle, the corner leads to a discontinuity in the manifolds. The turning points are not tent-like bending points, but points where the manifolds end. An example is an overlapping disk billiard, where the distance between the disk centers is less than the sum of the two radii. Scanning through the different outgoing angles starting in the corner gives a second pruning front which we denote as the corner pruning front, to distinguish it from the tangent pruning front obtained from the tangent singularity discussed above. The point corresponding to the orbit bouncing from the corner tangentially to the wall is common to the two pruning fronts. This is the end point for both kinds of fronts, and by using this point we can combine the two fronts into one.

7.2 3-disk

The three-disk system gives a complete horseshoe for some parameter values. In a symmetric system the horseshoe is complete when the distance r between the centers of the disks is sufficiently large. At some critical parameter value the non-wandering set becomes a not complete binary Cantor set, but to determine this critical parameter value is not trivial.

We want a condition on the geometrical construction of the non-wandering set to distinguish between sufficiently separated disks and the case of pruning. We find that the non-overlapping disks are sufficiently separated to realize a complete horseshoe if condition 1 below is true.

Definition: Λ_1^+ consists of M strips in the phase space, with each strip m^+ the union of initial points (x, ϕ) from which a trajectory starting at x with angle ϕ hits a particular disk. As such a trajectory might have to penetrate other disks, the M strips are not necessarily disjoint. Λ_1^- consists of the M strips, with each strip m^- the union of points (x, ϕ) where the trajectory starting at x with angle $-\phi$ hits a particular disk. We call a transverse intersection of a strip m^+ and a strip m^- a *rectangle*. The set $\Lambda_1 = \Lambda_1^+ \cap \Lambda_1^-$ then consists of M^2 rectangles, not necessarily disjoint. The set $\Lambda_T = \Lambda_T^+ \cap \Lambda_T^-$ with $T > 1$ consists of intersections of forward and backward strips corresponding to T consecutive bounces with the outgoing angle at each bounce equal to the incoming angle, but allowing the trajectories to go through discs. Then Λ_T consists of M^{2T} rectangles.

Condition 1 *There exists a finite integer T such that Λ_T consists of M^2 disjoint areas where each area is inside one of the M^2 rectangles of Λ_1 .*

The iteration of the M^2 disjoint areas corresponds to one more bounce and gives that each of the M^2 disjoint areas contains M^2 new disjoint areas. The M^4 rectangles of Λ_2 then contains M^4 disjoint areas. By induction we find that $\Lambda_{T+T'}$ gives $M^{2T'}$ disjoint areas inside the $M^{2T'}$ rectangles of $\Lambda_{T'}$. From this it follows that even if the rectangles of $\Lambda_{T'}$ overlap each other, the parts of the non-wandering set belonging to different rectangles do not overlap. A symbol string $(w_{-T'+1}w_{-T'+2} \dots w_{T'-1}w'_T)$, with $w_t \in \{0, 1, \dots, (M-1)\}$ corresponds to a unique rectangle, and is a substring of the symbol strings for all trajectories that pass through this rectangle. It then follows that the disks are sufficiently separated and the non-wandering set a complete horseshoe.

If the condition is not satisfied, there might be an infinitesimal change of the parameters that yields a finite $0 < T < \infty$; this is the critical parameter value where pruning starts. If such finite T cannot be realized for any perturbation of parameters, then the rectangles always overlap, and the symbol dynamics is always pruned.

A different and more intuitive way to describe the orbits that disappear first is to find the point in the Cantor set Λ in (x, ϕ) with the largest angle ϕ , and determine the parameter value for which $\phi = \pi/2$, i.e. this point represents an orbit bouncing tangential to a disk. In the symmetric three-disk system this point is the hetroclinic point where the unstable manifold of one period two orbit crosses the stable manifold of the other period two orbit. Numerically this can be found by starting an orbit grazing off the disc at the symmetry line and find the parameter value for which the orbit converges to the period two orbit. Figure 7.5 shows this orbit for the critical parameter value $r_c = 2.04821419 \dots$

There are two different homoclinic orbits that look like the orbit drawn in figure 7.5 for the critical parameter value r_c . For $r > r_c$ one of the orbits bounces off the disc, and the other orbit passes by the disk without bouncing for $r > r_c$. An orbit may then become singular either because a bounce gets an angle $\phi = \pi/2$ or because at a place without any bounce the path is grazing the disk. These orbits will define two pruning fronts for the non-overlapping dispersive billiards.

7.2.1 Pruning front

For $2 \leq r < r_c$ the above two pruning mechanisms give two forbidden regions in the symbol plane. We shall call the border of the regions the “tangential pruning front”. The two mechanisms are illustrated in figure 7.6. Figure 7.6 a) shows sections of two admissible orbits. One orbit passes by the dispersing wall, and the other one bounces off the wall from the dispersing side. Figure 7.6 c) shows corresponding

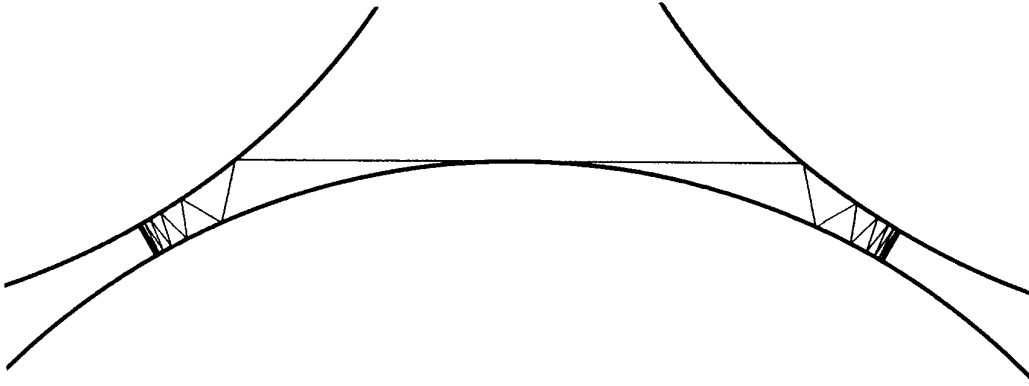


Figure 7.5: The hetroclinic orbit of the 3 disk system at the critical parameter value $r_c = 2.04821419\dots$ where this orbit bifurcates and becomes the first pruned orbit of the 3 disk system.

sections of two forbidden orbits. In one the trajectory penetrates the disk along a straight line. The other orbit bounces off the wall with the incidence angle θ larger than $\pi/2$, so the trajectory penetrates into the disc and bounces off the wall from the wrong side. The reason for including these unphysical orbits is that with them every n -ary alphabet symbol string is realized. The inadmissible orbits can be distinguished from the admissible orbits by observing that they include bouncing angles larger than $\pi/2$, or that the orbit goes through a wall. The singular limit orbit between the admissible and inadmissible orbits is the orbits tangentially to the wall, figure 7.6 b).

The pruning front can be calculated numerically by starting a tangential orbit at a point x on the disk, following the orbit through any number of bounces (in our numerical examples 30), and recording the corresponding symbol string. Given this future symbol string and the past symbol string obtained by bouncing tangentially off the disk in the opposite direction, we find for each initial $(x, \pm\pi/2)$ the corresponding symbol plane point (γ, δ) . As an orbit starting tangentially at a point x may be considered as the limit either of an orbit bouncing off the wall, or an orbit not touching the disk, we have two choices for the symbol s_0 . Either the symbol s_0 is the symbol corresponding to this disk and s_1 is the symbol of the next disk the particle bounces off, or we ignore the symbol of this disk and let s_0 be the symbol for the next bounce. In this way the tangent in phase space corresponds to two different pruning front points (γ, δ) in the symbol plane.

Assume (γ, δ) is the symbolic coordinate for an orbit bouncing tangentially off a disk. Then assume that the symbolic past is constant and change one symbol s_t in the future symbolic description. If the incidence angle for the corresponding orbit

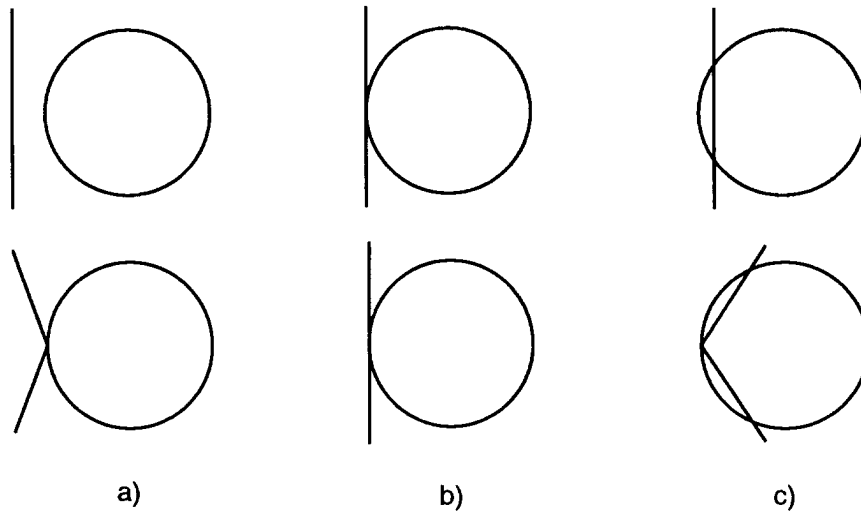


Figure 7.6: Orbit segments which are a) admissible, b) at the pruning point, and c) inadmissible. The two inadmissible orbits in c) are the only two pruning mechanisms for dispersive billiards without corners.

changes to $\phi > \pi/2$, this symbol string is pruned. It may also happen that the angle changes to $\phi < \pi/2$, in case which the orbit is admissible. The well-ordered symbols are constructed in such a way that an increase in the angle ϕ is an increase in the symbolic value, and in the well ordered symbol plane (γ, δ) , the symbolic representation of the tangent orbit is the border between the admissible and the pruned orbits i.e. the pruning front. An other important question is whether the front changes monotonously in the symbol plane. When we scan the different tangent orbits we increase monotonically the value of the position coordinate x , keeping the angle $\phi = \pi/2$ constant. As we move in the x -direction in the phase space we cross the foliation of both the stable and the unstable manifolds in only one direction. We then move monotonously in the space defined by the manifolds which is our symbol plane. The pruning front is obtained by the symbol strings from such a scan of x -values and is piecewise *monotone* in the symbol plane. The shifted symbol strings of these orbits are piecewise monotone, and we give examples of this in the figures below.

The second pruning front is given by the same symbolic string, except that the symbol for the tangential bounce is omitted. This pruning front then also has to be monotone. The second pruning front describes the orbits that do not bounce off the tangency disk and therefore has no representation in the symbol plane for this bounce. As any shift of the symbol strings is equivalent, we choose to draw

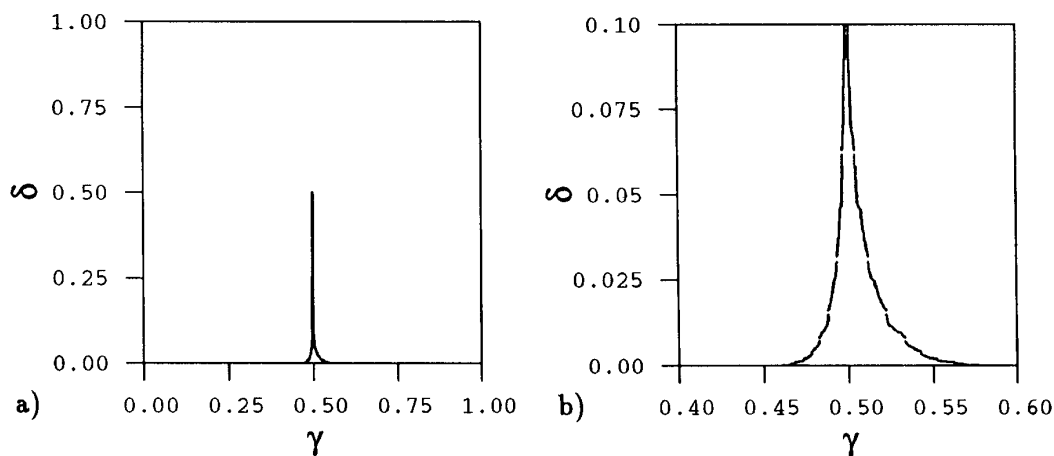


Figure 7.7: a) The tangent pruning front for the 3-disk system for touching disks, $r = 2$. b) Magnification.

both pruning fronts in the symbolic plane corresponding to the bounce immediately before the tangent bounce. These are of course also monotone curves. The region bounded by the two pruning fronts, from the two families of strings with and without the symbol of the tangent disk, and by the border of the unit square, is the *primary pruned region*.

Examples of the pruning fronts for the three-disk system are drawn in figures 7.7, 7.8 and 7.9.

We can numerically test the pruning front by plotting symbolic values (γ, δ) for a long chaotic orbit with random initial point. Such chaotic orbits are plotted in (γ, δ) in figures 7.10, 7.11 and 7.12. Comparing these with the pruning fronts of figures 7.7, 7.8 and 7.9 we see that the pruning front together with the edges of the symbol plane are the limites of white areas which are never visited by the chaotic orbits. We refer to the white area limited the pruning front as the primary forbidden region.

Beyond the primary forbidden regions, there are also other white areas in the figures. For figures 7.10 and 7.11 it follows from the conjecture of existence of only two pruning mechanisms for non-overlapping disks that all other white regions in the (γ, δ) plane are images or preimages of the primary regions. For example, it is easy to see that in figure 7.10 the largest visible white regions are around the lines $\gamma = 1/2^n$ and $\delta = 1/2^n$. The shift operation is a binary shift, so the large primary regions surrounding the lines $\gamma = 1/2$ and $\delta = 1/2$ are partly mapped into regions surrounding the lines $\gamma = 1/2^n$ and $\delta = 1/2^n$ because the shift operation make $\delta \rightarrow \delta/2$ if $\gamma < 1/2$, and similarly backward in time $\gamma \rightarrow \gamma/2$ if $\delta < 1/2$. At

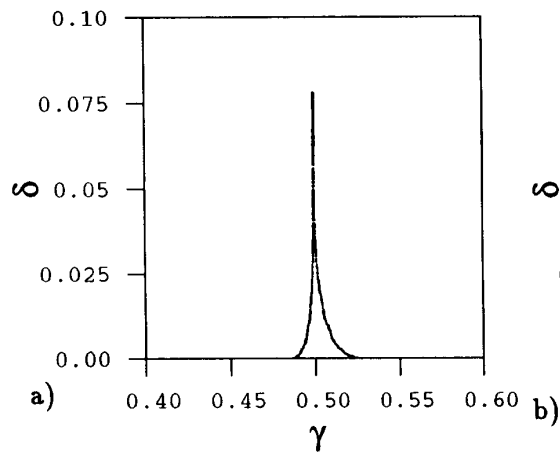


Figure 7.8: The tangent pruning front for the 3-disk scattering system $r = 2.02$.

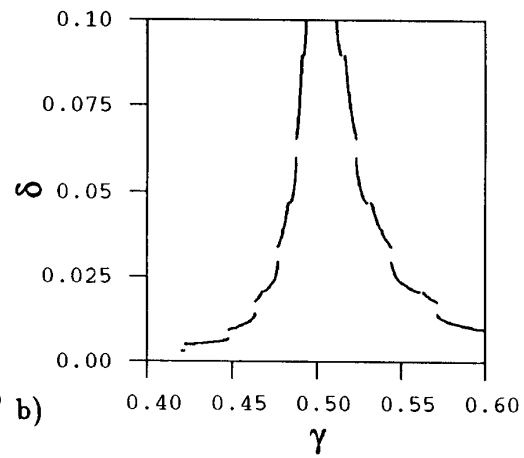


Figure 7.9: The tangent pruning front for the closed 3-disk system $r = 1.97$.

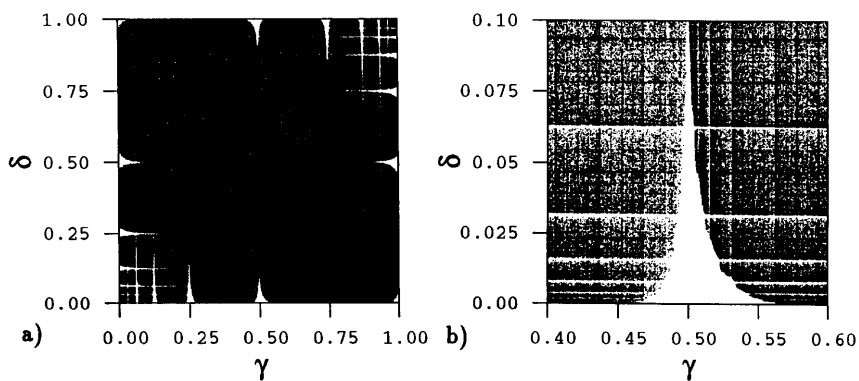


Figure 7.10: Bounces of a typical chaotic orbit plotted in (γ, δ) plane for the 3-disk system for touching disks, $r = 2$. b) Magnification of the primary pruned region.

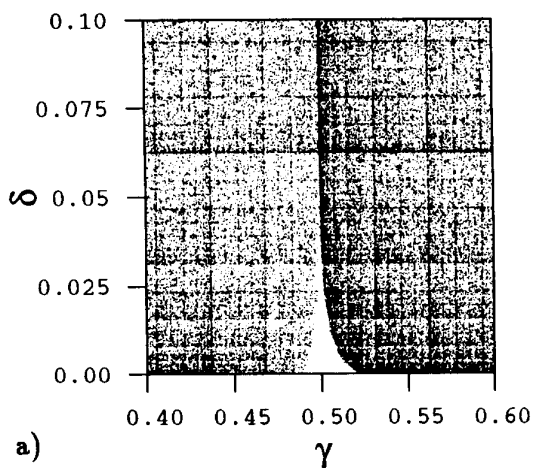


Figure 7.11: Bounces of a typical chaotic orbit plotted in (γ, δ) plane for the scattering 3-disk system, $r = 2.02$.

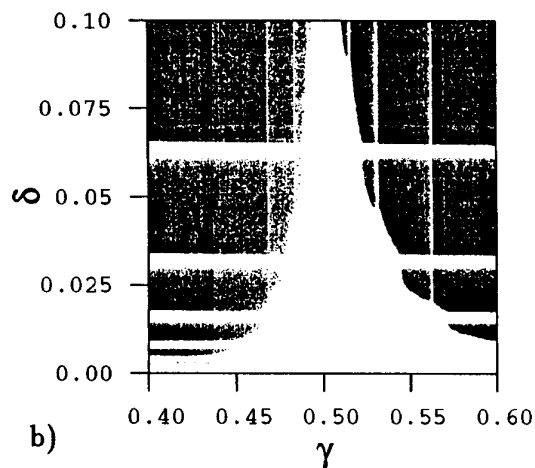


Figure 7.12: Bounces of a typical chaotic orbit plotted in the (γ, δ) plane for the closed 3-disk system, $r = 1.97$.

the same time the area is squeezed by a factor 2 in one direction and enlarged by a factor 2 in the other direction. As pointed out by Troll [193], this kind of well-ordered symbols has a more complicated time shift than the corresponding symbols s_t . For the s_t symbols the time shift is only a shift of the “present dot”, that is all indices t change to $t + \tau$ after τ iterations. In the (γ, δ) plane the time iteration is both a shift operation, and an inversion $\gamma \rightarrow 1 - \gamma'$ and $\delta \rightarrow 1 - \delta'$. This follows from the algorithm (6.7).

The more complicated time iteration is the price one has to pay to get symbols that have a simple spatial ordering. All systems for which there is a change in direction under the folding cannot be ordered in space and time simultaneously.

The area of the primary pruned region grows as the parameter r decreases in the symmetric 3-disk system. As the distance between the disks becomes smaller, more and more orbits become forbidden, and the pruning front moves enlarging the pruned region. The topological entropy then decreases as r decreases.

7.2.2 Overlapping disks

In the 3-disk system with $r < 2$ the disks overlap each other. This leads to an additional pruning front mechanism. As long as the disks are not overlapping each other an orbit can bounce an arbitrarily number of times close to the period 2 cycle $\overline{s_1 s_2} = \overline{12}$ or $\overline{23}$ or $\overline{31}$, in the well-ordered symbols close to either $\overline{w_1} = \overline{0}$ or $\overline{w_1} = \overline{1}$. When the disks touch each other, $r = 2$, the cycle $\overline{s_1 s_2} = \overline{10}$ disappears, and for overlapping disks, $r < 2$, an orbit can only have a finite number of bounces

in a corner where two disks intersect. How many times a particle can bounce in the corner depends on the angle at which it arrives to the corner. The corner pruning front is obtained by bouncing out from the corner at all allowed angles, and determining the corresponding symbolic values (γ, δ) .

The corner pruning front is drawn in figure 7.13 for $r = 1.9$. The tangential pruning front for the same parameter value is drawn in figure 7.14. In figure 7.15 we have drawn the two pruning fronts and some of their images together; we note that the corner pruning front ends where the tangent pruning front starts. A long chaotic orbit, figure 7.16, stays below the pruning front and never crosses into the forbidden white regions.

The corner pruning front moves down and gives a larger forbidden region as the disks move together. Figure 7.17 shows the corner pruning front for the parameter value $r = 1.8$, and figure 7.18 shows the tangent pruning front for the same parameter value. The corner pruning front becomes more important as r decreases and the tangent pruning front becomes smaller as r decreases.

In the limit where the area of the domain in which the particle bounces vanishes ($r \rightarrow \sqrt{3} = 1.732\dots$) the domain approaches a triangle, and the tangential pruning front shrinks to a point, the point common to the two pruning fronts. As we show in chapter 8, the corner pruning front becomes a straight line.

7.2.3 Approximating the pruning front

The pruning front is an exact solution to the problem of “which orbits are forbidden in the billiard system”, limited only by the numerical accuracy of calculating an orbit.

This picture is neither less nor more useful than the kneading sequence of the logistic map. To be useful in calculations of average values of physical interest the primary forbidden region has to be transformed into a description of admissible orbits in such a way that one can construct the Markov diagrams and the associated zeta function expansions for the new symbolic alphabet.

There may be several ways to do this but, we have chosen to follow the same procedure that we have used for one-dimensional maps. The forbidden region can be split into rectangles described by finite symbol strings which corresponds to paths of finite length down the symbolic tree, and we construct an approximate sequence of finite Markov graphs or automata. In the unimodal map this procedure works very well, and for the Hénon map it will converge rather well. The procedure also works in the billiards studied here, but the convergence has to be less good as the pruning front does not have a staircase structure as the Hénon map, with

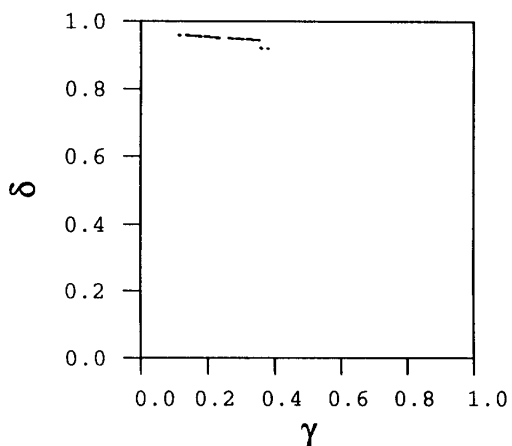


Figure 7.13: The corner pruning front for 3 overlapping disks, $r = 1.9$.

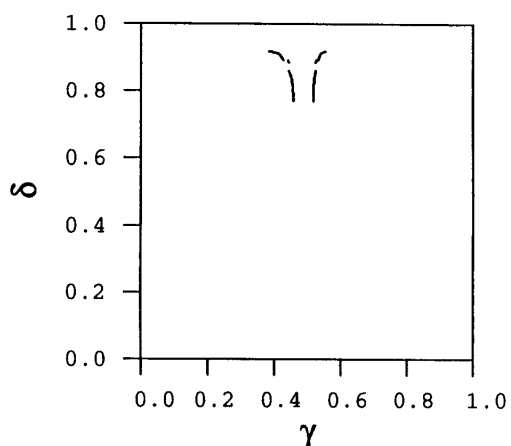


Figure 7.14: The tangent pruning front for 3 overlapping disks, $r = 1.9$.

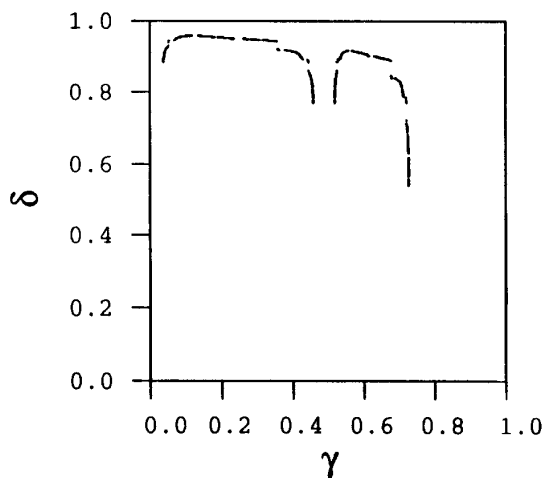


Figure 7.15: The corner pruning front, the tangent pruning front, together with some of their images, $r = 1.9$.

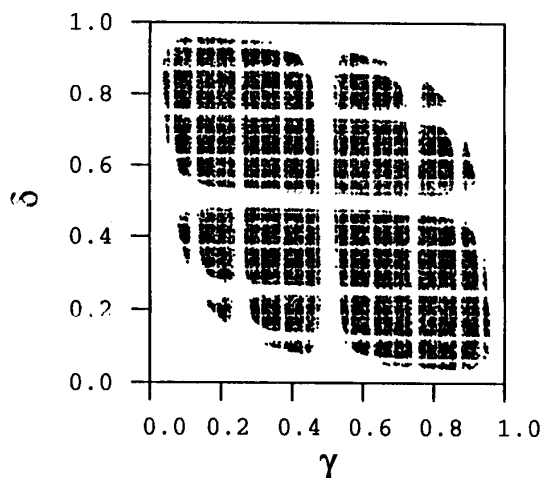


Figure 7.16: Bounces of a long chaotic orbit for the 3 overlapping disks, $r = 1.9$.

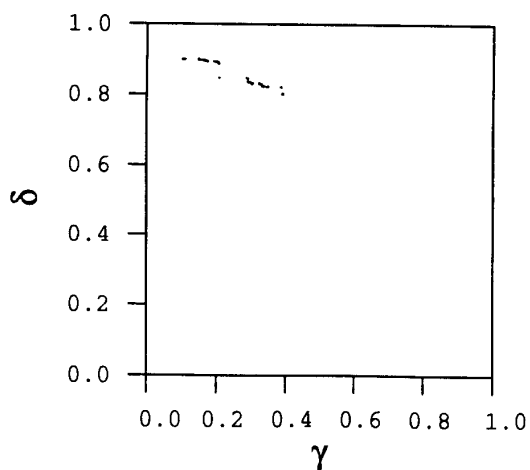


Figure 7.17: The corner pruning front for 3 overlapping disks, $r = 1.8$.

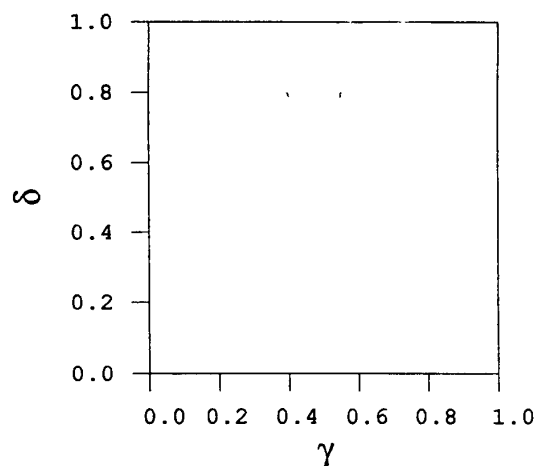


Figure 7.18: The tangent pruning front for 3 overlapping disks, $r = 1.8$.

a few large steps and smaller steps organized in a hierarchy. For a staircase-like pruning front where the steps become small very fast, a few rectangles cover most of the forbidden regions. If the pruning front is more like a smooth curve, the approximation with rectangles converges slowly. This suggests that we should use some kind of trapezoidal approximation, but at present we do not know how to implement this.

The first step is to find the forbidden rectangles in the symbol plane (γ, δ) . In figure 7.19 we draw the pruning front together with a staircase approximation with steps at all rational values $p/2^7$. If we make an “under-pruning” (“under-counting”) approximation where we let the approximating curve be entirely inside the forbidden region. We then take away too few of the forbidden orbits, but we are guaranteed that any orbit that exists in the system will be included in the new alphabet we construct. Alternatively we can choose to “over-prune” and let the approximation be on the other side of the pruning front. This implies that there are orbits in the system which cannot be represented in the alphabet we construct but every symbol sequence generated is realized by the dynamics. The third possibility is to choose a “closest” curve which partly over-prunes and partly under-prunes the system.

The approximation curve in figure 7.19 is an under-pruning curve, including some squares which are completely in the forbidden region. Each square with the side length 2^{-k} corresponds to a symbol string of length $2k$ in the symbolic description. The forbidden symbol strings of lengths 12, 14, 16, and 18 are given in table 7.1.

As an example, we implement this by taking the shortest forbidden string which

$_{-}w_{-5} \dots w_{6-}$	$_{-}w_{-6} \dots w_{7-}$	$_{-}w_{-7} \dots w_{8-}$
000000 · 100000	0000000 · 1000011	00000000 · 10001010
	0000000 · 1000010	00000000 · 10001001
	0100000 · 1000001	00000000 · 10001000
	0100000 · 1000000	01000000 · 10000101
	1100000 · 1000000	01000000 · 10000100
	0010000 · 1000000	11000000 · 10000100
	1000000 · 0111111	01100000 · 10000010
	0000000 · 0111111	11100000 · 10000010
	0000000 · 0111110	01010000 · 10000001
	0100000 · 0111111	01010000 · 10000000
		11010000 · 10000000
		00110000 · 10000000
		10110000 · 10000000
		01110000 · 10000000
		11110000 · 10000000
		00001000 · 10000000
		01010000 · 01111111
		10010000 · 01111111
		00010000 · 01111111
		11100000 · 01111111
		01100000 · 01111111
		01000000 · 01111101
		00000000 · 01111011

Table 7.1: The forbidden orbits in 3 discs, $r = 2$. “Under-counting” approximation to level 9.

$_{-}w_{-8} \dots w_{9-}$		
000000000 · 011110011	110101000 · 100000000	001000000 · 100001110
000000000 · 011110100	010101000 · 100000000	001000000 · 100001111
000000000 · 011110101	100101000 · 100000000	110000000 · 100010000
100000000 · 011110101	000101000 · 100000000	010000000 · 100010000
010000000 · 011110111	111001000 · 100000000	010000000 · 100010001
001000000 · 011111000	011001000 · 100000000	000000000 · 100010110
001000000 · 011111001	101001000 · 100000000	000000000 · 100010111
011000000 · 011111011	001001000 · 100000000	000000000 · 100011000
111000000 · 011111011	110001000 · 100000000	000000000 · 100011001
000100000 · 011111011	010001000 · 100000000	
001100000 · 011111101	000110000 · 100000010	
101100000 · 011111101	111010000 · 100000010	
011100000 · 011111101	011010000 · 100000010	
111100000 · 011111101	011010000 · 100000011	
011010000 · 011111110	010010000 · 100000100	
011010000 · 011111111	100010000 · 100000100	
111010000 · 011111111	000010000 · 100000100	
000110000 · 011111111	000010000 · 100000101	
100110000 · 011111111	001100000 · 100000110	
010110000 · 011111111	010100000 · 100001000	
110110000 · 011111111	100100000 · 100001000	
001110000 · 011111111	000100000 · 100001000	
101110000 · 011111111	000100000 · 100001001	
011110000 · 011111111	111000000 · 100001010	
111110000 · 011111111	011000000 · 100001010	
000001000 · 011111111	001000000 · 100001100	
100001000 · 011111111	001000000 · 100001101	

Table 7.1: Continue.

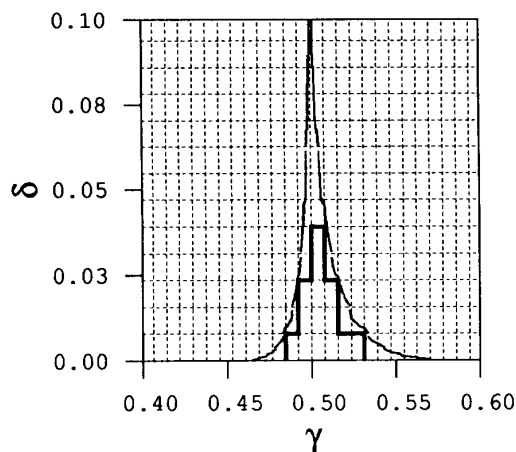


Figure 7.19: The pruning front for the 3 disk system for touching disks, $r = 2$, and a rational rectangles approximation.

has length 12, together with the time reversed version of the string and the conjugate strings (0 and 1 interchanged) as the forbidden strings which we remove from the binary tree. The corresponding Markov diagram is too complicated to implement by hand, and we use a computer program that generates an automaton from a list of forbidden strings. In order to handle the tree structure this program has to be relatively complicated; because of the object oriented structure of the data we have programmed it in C. The nodes with pointers to other nodes are programmed as *struct* variables, with pointers containing the address of the variables. The construction of the automaton is quite fast, but going through all loops and finding all possible combinations of non self-intersecting loops can be time consuming. We find that when the number of nodes in the automaton is larger than a number between 50 and 100, the time the program needs to scan all loops is too large for practical calculations. This may however vary a lot depending on the number of symbols and the structure of the automaton.

The result of this calculation is the fundamental part of the zeta function with all the terms that are not shadowed by shorter orbits but usually also a number of orbits that are shadowed together with the shadowing combinations. We will return to this problem in chapter 11. If we were only interested in determining the topological entropy, section 1.3, we could simply find the average number of symbol strings of a given length starting at one node in the tree. In practice this converges rather quickly with the length of the string to the correct entropy and can be applied to rather large trees.

With the 4 pruned symbol strings of length 12; 000000100000, 000001000000,

111111011111, 111110111111, we obtain an automaton with 35 nodes and the longest loop of length 22. The topological polynomial is

$$\begin{aligned}
 p(z) = & (-1 + z)^2 (1 + z) (1 - z + z^2) \\
 & (1 + z + z^2) (1 + z^6 + z^7 + z^8 + z^9 + z^{10} + z^{11}) \\
 & (1 - z - z^2 - z^3 - z^4 - z^5 - z^6 - z^8 - 2z^9 - 3z^{10} \\
 & - 4z^{11} - 3z^{12} - 4z^{13} - 3z^{14} - 2z^{15} - z^{16})
 \end{aligned} \tag{7.1}$$

The 4 forbidden strings are symmetric under time reversal and $0 \leftrightarrow 1$ interchanged so we expect that the polynomial can be factorized [48]. The leading zero belongs to the 16th order polynomial, and yields $h = \ln 1.99856 \dots$

The automaton can also be constructed with all the length 12 and 14 forbidden symbol strings, table 7.1. Some of the forbidden strings can be reduced to shorter strings; e.g. the two strings of length 14, 0000000 · 1000011 and 0000000 · 1000010, can be combined to one length 13 string 0000000100001, and both the two strings 0100000 · 1000000 and 1100000 · 1000000 contain the forbidden length 12 string 000001000000 and can be left out from the list. All strings up to length 14 are pruned by the following list of forbidden strings

$$\begin{aligned}
 & 000000100000 \\
 & 0000000100001 \\
 & 0100000100000 \\
 & 0000000111111 \\
 & 0000000011111 \\
 & 00100001000000 \\
 & 01000000111111
 \end{aligned} \tag{7.2}$$

together with the time reversed strings and the strings with 0 and 1 interchanged. These forbidden strings yield an automaton with 171 nodes, too large for determination of all non-intersecting loops and their combinations. Counting all possible paths from the root node gives a topological entropy estimate $h = \ln 1.99575 \dots$

That the calculation exceeds our computational skills after just a few approximations may seem discouraging, but the touching disk example is a bit special among the pruned systems because it has very few forbidden strings, or more precisely; there are no short orbits which are pruned. The average number of symbols is around 1.99 which is rather close to 2, and the pruning is not so important as in many other systems. The method works much better in the cases with heavy pruning and where one really needs to control pruning in order to apply the theory to problems such as evaluation of semiclassical resonances.

For the overlapping three disk problem, e.g. $r = 1.9$, we find more interesting results. We can draw the pruning front for the corner and tangent pruning together with a 2^{-k} lattice and find the symbols corresponding to squares outside the pruning front in the forbidden region. By combining the forbidden strings we obtain the following list of forbidden orbits up to length 12:

$$\begin{aligned}
 &11111 \\
 &1101111 \\
 &11110000 \\
 &11100000 \\
 &110111011 \\
 &101111010 \\
 &111011101 \\
 &1111010111 \\
 &11011011101 \\
 &001111010111 \\
 &101111001111
 \end{aligned} \tag{7.3}$$

Pruning the two strings 11111 and 00000 of length 5 yields an automaton with 9 nodes and the characteristic polynomial

$$p(z) = (1 - z - z^2 - z^3 - z^4) (1 + z + z^2 + z^3 + z^4) \tag{7.4}$$

with a topological entropy $h = \ln 1.927561\dots$

Pruning the strings of length 5 and 7 yields an automaton with the characteristic polynomial

$$\begin{aligned}
 p(z) = &(-1 + z + z^2 + z^3 + z^4 - z^5 + z^6 - z^7 - z^{10}) \\
 &(-1 - z - z^2 - z^3 - z^4 - z^5 - z^6 + z^7 + 2z^8 + 2z^9 + z^{10})
 \end{aligned} \tag{7.5}$$

giving a topological entropy $h = \ln 1.893040\dots$. Including also the length 8 forbidden strings yields an automaton with 31 nodes with

$$\begin{aligned}
 p(z) = &(1 + z + z^2 + z^3 - 2z^7 - 2z^8 - 2z^9 - z^{10}) \\
 &(1 - z - z^2 - z^3 - 2z^6 + z^{10})
 \end{aligned} \tag{7.6}$$

which yields the topological entropy $h = \ln 1.889286\dots$. The value of e^h as a function of the maximal length of the forbidden strings included is plotted in figure 7.20 a). The topological entropy seems to converge to $h = \ln 1.862\dots = 0.62\dots$. We can plot the values $\ln(z - z_{l=12})$ as a function of the length as we did for the logistic map in figure 1.23. For the logistic map we found that this plot was linear with a slope $-h$. In figure 7.20 b) the convergence of the entropy seems to be faster as a function of the length of the forbidden strings. If the few points plotted are approximated by a line the slope is around -1 .

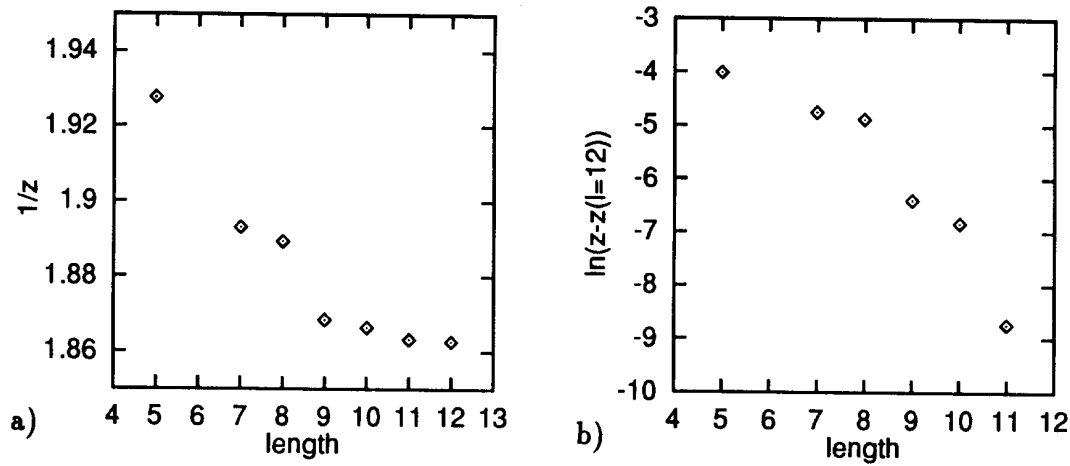


Figure 7.20: The values a) $a/z = e^h$ and b) $\ln(z - z_{l=12})$ as a function of the length of the forbidden strings for 3 disk $r = 1.9$.

7.3 4-disk

The analysis of the symmetric four disk system is very similar to the three disk system. We construct pruning fronts from the tangential and the corner orbits, and find the forbidden regions in the symbolic value plane (γ, δ) . The alphabet s_t has 4 symbols, and the well-ordered alphabet, eq. (6.12), has 3 symbols. Hence the symbolic values are base-3 numbers, and the shift operations looks slightly different from the binary 3-disk case.

As for the three-disk system, the pruning starts at a critical disk separation r_c , where a point in the non-wandering set attains $\theta = \pi/2$. This outermost point is the hetroclinic point where the unstable manifold of one period-2 orbit, e.g. $\overline{s_1 s_2} = \overline{12}$, crosses the stable manifold of another period 2 orbit, e.g. $\overline{s_1 s_2} = \overline{23}$. We find numerically $r_c = 2.20469453 \dots$. Hence for the 4-disk system the pruning starts when the distance between the disks is approximately 20% of the radius, while in the 3-disk system pruning started at the distance approximately 5% of the radius.

For $2 \leq r < r_c$ the forbidden regions are limited by the tangential orbit pruning fronts. Figure 7.21 shows the pruning front for the touching disk case, $r = 2$.

As for the three-disk system, we make a grid in the symbol plane, and read off the forbidden strings listed in table 7.2.

The shortest forbidden string is the length 6 string 000100 (in terms of the w_t symbols) and letting this sting and the symmetric strings 001000, 222122 and 221222 be forbidden we obtain an under-pruned Markov graph with a new alphabet

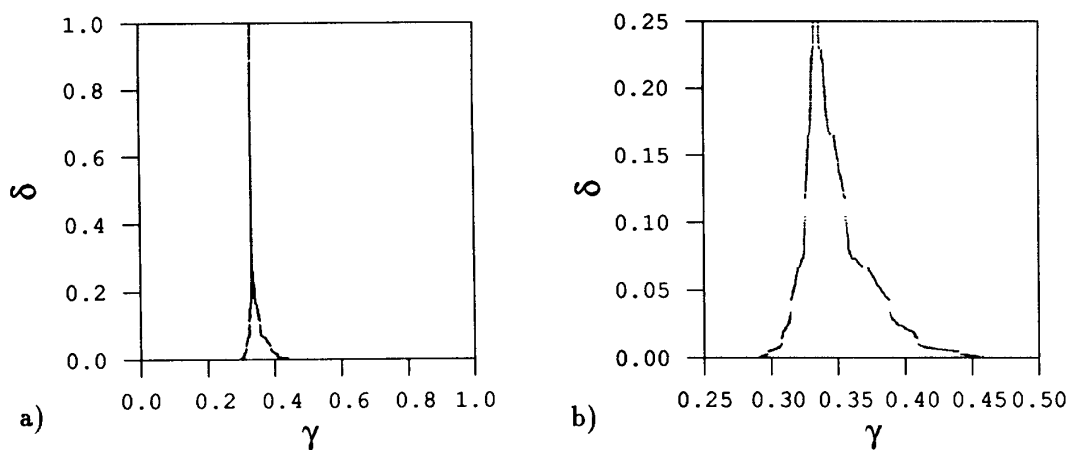


Figure 7.21: The pruning front for the touching 4-disk system, $r = 2$. b) Magnification.

and the characteristic polynomial

$$p(z) = (-1 + z)^2 (1 + z) (1 + z + z^2) (-1 + z - z^2 - z^4) \quad (7.7)$$

$$(-1 + 2z + 2z^2 + 2z^3 + z^4 + 3z^5 + 3z^6 + 3z^7 + z^8) \quad (7.8)$$

with the topological entropy $h = \ln 2.986497\dots$

We can also approximate the pruning front with the symbol strings from the squares which are mostly in the forbidden region. This gives the strings 00100, 000022 and 000101 and the symmetric ones of these and we obtain an automaton with 34 nodes and with topological entropy $h = \ln 2.95302\dots$

We can find all completely forbidden strings of length less or equal 8 and by combining the forbidden strings in table 7.2 we get the list of forbidden strings

$$\begin{aligned}
 &000100 \\
 &0000101 \\
 &0000222 \\
 &0001010 \\
 &0010010 \\
 &0010011 \\
 &00000221 \\
 &00010110 \\
 &01000222 \\
 &01001010 \\
 &11000222 \\
 &10001011
 \end{aligned} \quad (7.9)$$

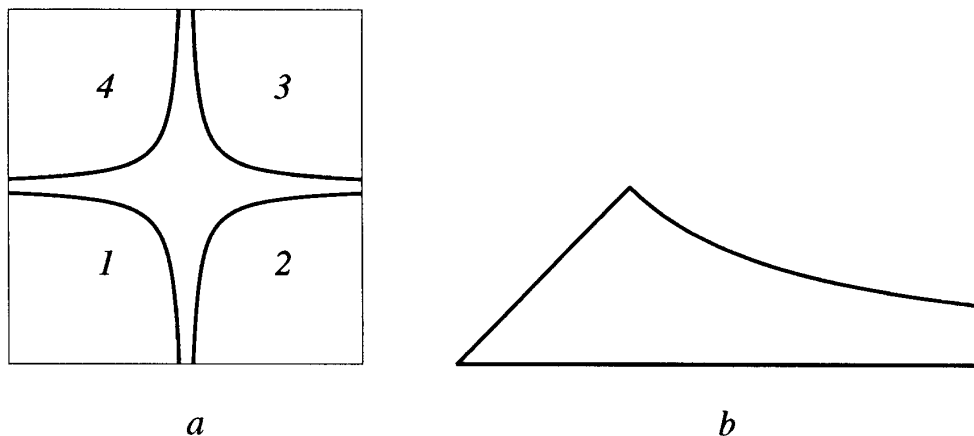


Figure 7.22: The hyperbola billiard. a) The full configuration space. b) The fundamental domain.

Including stings up to length 7 gives $h = \ln 2.96914\dots$ and also including the strings of length 8 gives $h = \ln 2.96519\dots$. The automaton in this case has 135 nodes and it is very time consuming to find all loop combination in the graph.

The topological entropy is close to the topological entropy of a three letter alphabet $h = \ln 3$, but the pruning is larger for the 4 disk touching system than in the 3 disk touching system.

7.4 Hyperbola billiard

The hyperbola billiard is a system similar to the 4 disk system where a point particle bounces elastically between the four hyperbola branches

$$y = \pm \frac{1}{x} \quad (7.10)$$

drawn in figure 7.22 [15, 176, 177, 178]. The symmetry in this billiard is the same as for the 4 disk system and the walls are dispersing. A pruning front for this system can be obtained in the same symbol plane as the 4 disk system. The four hyperbolas are enumerated s_t counterclockwise and (6.12) and (6.13) gives the well ordered symbols and the coordinate (γ, δ) . As for the touching 4 disks the periodic orbit $\bar{w} = \bar{0} = \bar{1}$ does not exist. The walls does not overlap giving a corner and the tangent orbits are the only singular orbits in the system. The tangent pruning fronts give the pruned regions in (γ, δ) and are drawn in figure 7.23.

The tangent pruning fronts are the same two fronts as for the disk systems; one for the primary pruned region of orbits bouncing in the wall from the wrong

$w_{-2} \dots w_{3-}$	$w_{-3} \dots w_{4-}$
000 · 100	0000 · 0221
	0000 · 0222
	1000 · 0222
	2000 · 0222
	0100 · 0222
	1100 · 0222
	0100 · 1000
	1100 · 1000
	2100 · 1000
	0200 · 1000
	1200 · 1000
	2200 · 1000
	0010 · 1000
	1010 · 1000
	2010 · 1000
	0110 · 1000
	0200 · 1001
	2100 · 1001
	1100 · 1001
	0100 · 1001
	1100 · 1002
	0100 · 1002
	0100 · 1010
	2000 · 1010
	1000 · 1010
	0000 · 1010
	1000 · 1011
	0000 · 1011
	0000 · 1012

Table 7.2: The forbidden orbits in 4 discs, $r = 2$. Under counting approximation to level $k = 4$.

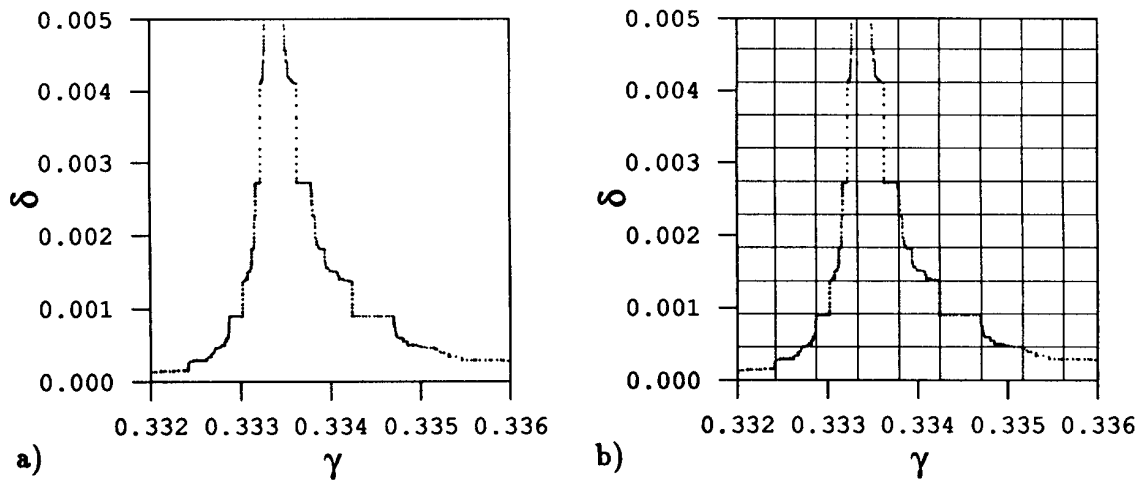


Figure 7.23: A magnification of the pruning front of the hyperbola billiard. b) with a lattice of size 3^{-7}

side and one region for orbits going through a wall without bouncing. We find in figure 7.23 that the primary pruned region is small compared with the touching 4 disk system. Qualitatively the shape of the front is slightly different than what we find in the disk billiards; the front has a more visible step-like shape. This may be because compared to the disk systems here more of the pruning is close to the origin and there is less pruning out in the tails $x \rightarrow \pm\infty$ and $y \rightarrow \pm\infty$.

To obtain lists of forbidden orbits of finite length we draw a lattice with length 3^{-k} between the lattice lines as in figure 7.23 b) and find the symbolic description of the rectangles in the forbidden region. This gives the following list of forbidden

orbits with symbol strings w_t shorter or equal 15.

$$\begin{aligned}
 &0000001000000 \\
 &0000001000001 \\
 &0000000100000 \\
 &1000000100000 \\
 &00000000222222 \\
 &00000001000010 \\
 &10000001222222 \\
 &00000000100001 \\
 &10000002222222 \\
 &00000002222222 \\
 &00000002222221 \\
 &000000000222221 \\
 &000000002222210 \\
 &010000010000010
 \end{aligned} \tag{7.11}$$

and the strings symmetric to these. The shortest forbidden string is of length 13 and the pruning is very small in this system. By pruning these strings we get an automaton with 270 nodes and a topological entropy

$$h = \ln 2.999972 \dots$$

This entropy is very close to $h = \ln 3$ as for a complete three letter alphabet. It was also noticed by Sieber [176] that the number of periodic orbits missing in a three letter alphabet is very small. In practical calculations a three letter alphabet can be used with small errors even though a random infinite string of symbols has a probability 1 that it is forbidden because a random string would sooner or later contain one of the forbidden strings in the list.

7.5 6+1 Disk system

We can also construct the pruning fronts for the system with one disk surrounded by 6 disks in figure 7.24. In this system the pruning starts already when the distance between the disc centers is $r_c = 3.59148407 \dots$, and we expect large pruning when the disks are close. There are two different tangent pruning fronts; one from orbits tangent to the center disk and one from orbits tangent to one of the other disks. The center-disk pruning front gives the largest pruned region. When the disks touches each other for $r = 2$ the system is reduced to 6 independent closed 3 disk systems and we do not have any corner pruning front for $r \geq 2$.

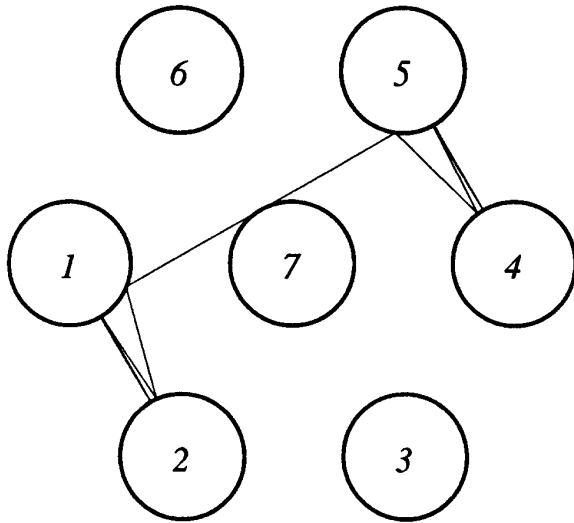


Figure 7.24: The 6+1 disk system and a hetroclinic orbit at the critical parameter value $r_c = 3.59148407\dots$

The well ordered symbols and the symbolic coordinate (γ, δ) are given by (6.18) and (6.19). The (γ, δ) space we use are the one corresponding to the phase space of a bounce in one of the 6 surrounding disks. The phase space for the center disk is different and we choose not to work in (γ, δ) for this disk. The pruned regions looks different in this space because the regions here are complicated shifts of the regions in the other symbol space.

The symbolic values γ and δ are base 5 numbers and a lattice with length 5^k between the lattice lines gives squares corresponding to symbol strings of length $2k$. The pruning fronts for the 6+1 disk system with parameter $r = 2.2$ are drawn in figure 7.25. From this picture we get the following list of forbidden strings:

$$\begin{array}{lll}
 31 & 420 & 4220 \\
 41 & 320 & 3220 \\
 & 421 & 1213 \\
 & 321 & 1214 \\
 & 221 & 0213 \\
 & 113 & 0214 \\
 & 114 & 1010 \\
 & 013 & 0010 \\
 & 014 & 0011
 \end{array} \tag{7.12}$$

and the time reversed and $4 - w$ reversed of these stings.

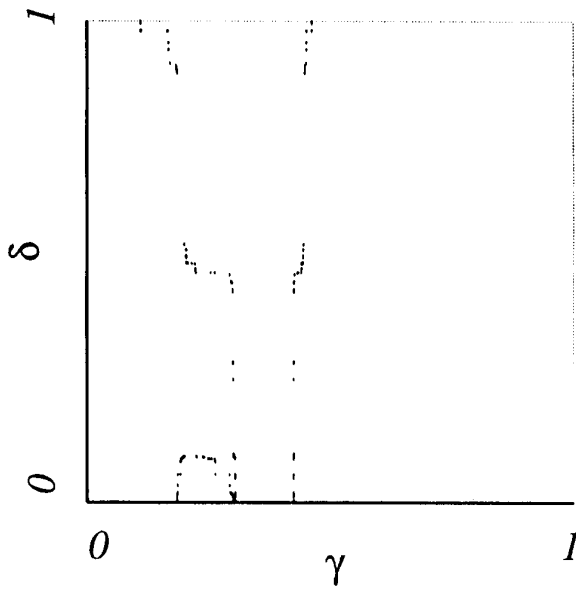


Figure 7.25: The pruning front of the 6+1 disk system for $r = 2.2$.

The forbidden strings up to length 4 gives an automaton with 33 nodes and a topological entropy

$$h = \ln 3.131\dots \quad (7.13)$$

which is much lower than the well separated 6+1 disk system where $h = \ln 5$. This is an example where the pruning is very important for the description of the system.

7.6 Stadium billiard

We have different well ordered alphabets describing the stadium billiard and a corresponding symbols plane (γ, δ) for each alphabet as discussed in section 6.5. In each (γ, δ) we will have a monotone pruning front and we can identify forbidden strings of increasing length. All different symbol planes will in principle give pruned regions consisting of the same strings when translated into the same alphabet. The approximation to a given length k of the strings w_t for the pruned region may yield slightly different results for the different alphabets. When constructing the new alphabets the different combinations of symbols imply that a square of the symbol plane may correspond to different lengths of the strings in the different alphabets.

In the non overlapping disk systems there were two kind of forbidden orbits, orbits going into the disk and bouncing from the wrong side and orbits going through a disk without bouncing. By including these unphysical orbit we have a complete

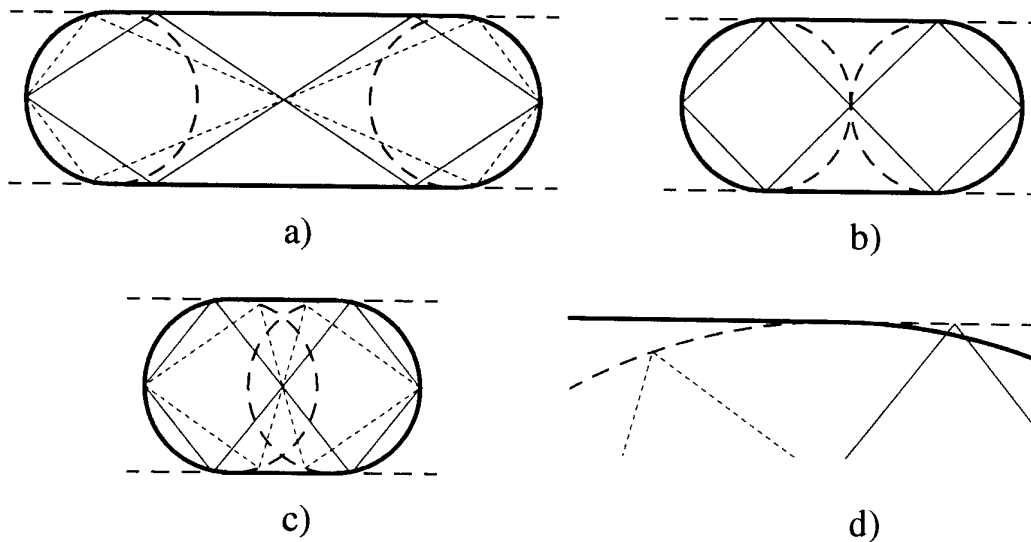


Figure 7.26: The orbits with s^a symbols $\overline{111333}$ and $\overline{012032}$ for a) $a = 2$, b) $a = 1$, c) $a = 0.6$. d) is a Blow-up of c).

n -ary symbolic description of all orbits. It is shown by Biham and Kvale [25] that in a similar way one can find unphysical orbits in the stadium billiard. These are the orbits that bounce in the straight line outside the singular point where the straight line joins the semi-circle, and the orbits which bounce in the circle inside the billiard domain. By including these unphysical orbits we can find all orbits described by the symbols obtained from the Markov graphs in section 6.5.

When we decrease the length a of the straight line in the billiard we have bifurcations. The bouncing points of an orbit with a given symbolic description may move as a decreases, and a points where the particle bounces off a wall moves closer to the closest singular point. In figure 7.26 we show one example of two orbits that become forbidden when a decreases below a critical parameter value; $a_c = 1.0$.

The orbit drawn with dashed lines in figure 7.26 is the orbit described with symbols s^a : $\overline{111333}$ or $\overline{444555}$ with s^b : $\overline{111333}$ or $\overline{444555}$ with s^c : $\overline{022011}$ and with s^d : \overline{eac} . The orbit drawn with solid lines is the orbit described with symbols s^a : $\overline{012032}$ or $\overline{240250}$ with s^b : $\overline{012032}$ or $\overline{210230}$ with s^c : $\overline{404303}$ and with s^d : \overline{ghf} .

These strings can be found as paths in the Markov graphs in figures 6.23, 6.24 and 6.25 and exist in the limit of an infinite long stadium $a \rightarrow \infty$. In figure 7.26 a) we find that the two orbits also exist when $a = 2$ but for $a = 0.6$ in figure 7.26 c) and d) these two orbits bounces off the illegal part of the stadium. The orbit \overline{eac} bounces off the circle on the wrong side of the singular point inside the stadium where the semi-circle does not exist and the orbit \overline{ghf} bounces off the straight line

outside the singular point where a physical orbit would bounce in the semi-circle. Figure 7.26 b) shows that for $a = 1$ the two orbits bounce exactly off the singular point and are on the limit of being illegal. These orbits are on the pruning front for $a = 1$. Biham and Kvale have numerically found periodic orbits and checked if each orbit is bouncing off the legal or forbidden part of the walls of the stadium.

We can draw the pruning front by finding the symbolic description of all orbits bouncing in the singular point with different outgoing angles. We record the symbol string as the symbols s^a and can translate these to the symbol space we want to use. The pruning front is drawn in (γ^a, δ^a) for the parameters $a = 5$, $a = 1$ and $a = 0.5$ in figure 7.27. The pruning front is also drawn in the (γ^b, δ^b) plane in figure 7.28 for these parameter values. As a check of the pruning front we have drawn the symbolic values of $1.5 \cdot 10^6$ bounces of chaotic orbits in the stadium with $a = 1$ in figure 7.29 for (γ^a, δ^a) and in figure 7.30 for (γ^b, δ^b) . The pruning fronts are exactly the border of the points in these figures.

We can make a lattice with separation 5^{-k} between the lattice lines and read off the symbol strings that are forbidden in the primary pruned region which is not forbidden for $a \rightarrow \infty$. This gives the list in table 7.3 for $k = 2$ where we give all strings w^b and some of the corresponding strings s^b . In addition there is the strings of s^b symmetric to the given ones. The choice of approximating the pruning front in either symbol plane (γ^a, δ^a) or (γ^b, δ^b) does not make any other difference than changing the order in which we find the forbidden substrings when increasing k .

7.7 Wedge billiard

The pruning front in the wedge billiard is obtained by the symbol plane representation of the singular orbits from the tip of the wedge. For the two bouncing ball system these orbits are the points where the balls bounces together and in the floor simultaneously. In the map (6.22) the singular orbits are point on the line $(x_t - 2y_t)^2 \cos^2 \theta + y_t^2 \sin^2 \theta = 1$ which is the border between map T_0 and map T_1 .

The pruning front is drawn in figure 7.31 for parameter values a) $\theta = 50^\circ$, b) $\theta = 60^\circ$, c) $\theta = 70^\circ$ and d) $\theta = 80^\circ$. The pruning fronts can be compared with figure 7.32 where we have plotted each bounce of a chaotic orbit with 10^6 iterations. The bounces are plotted in the symbol plane (γ, δ) . These figures show that the pruning front is the border of the primary pruned region.

The primary pruned region changes as the parameter changes, but in contrast to the examples above there is not a monotone increase in the area of the region. In the limit $\theta = 45^\circ$ most of the forbidden orbits are obits in the upper left corner.

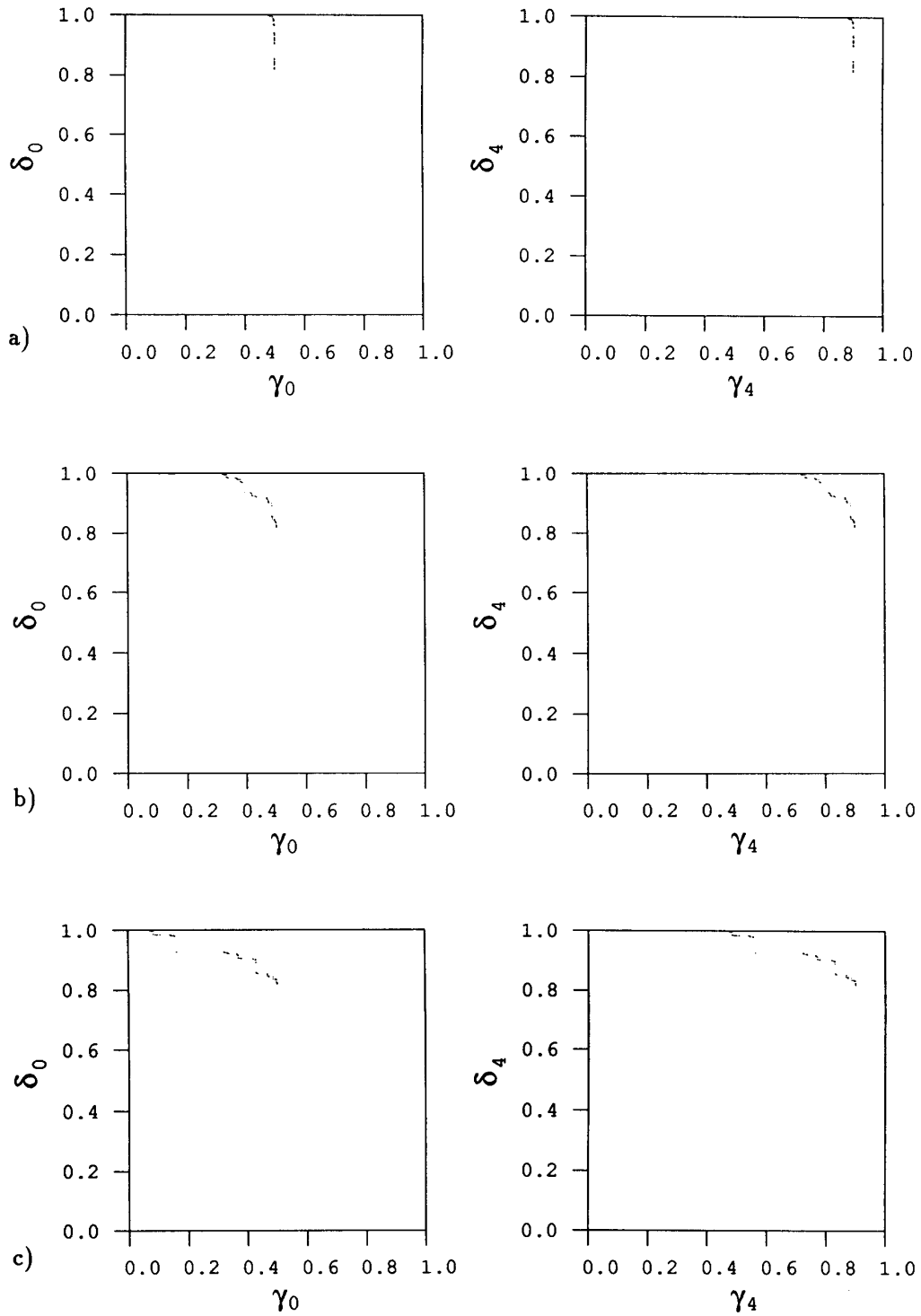


Figure 7.27: The pruning front for the stadium in the (γ^a, δ^a) symbol plane a) $a = 5$, b) $a = 1$, c) $a = 0.5$.

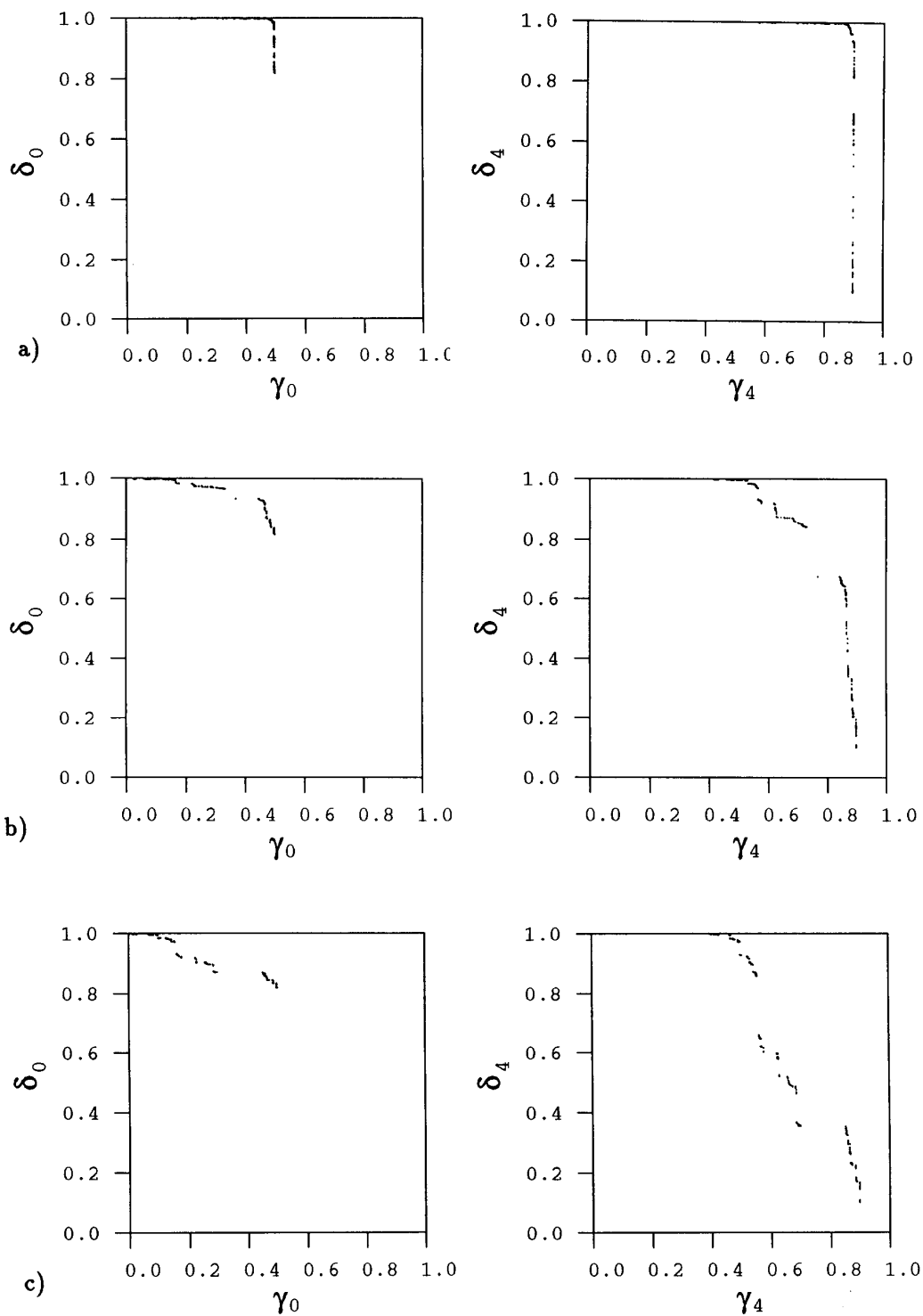


Figure 7.28: The pruning front for the stadium in the (γ^b, δ^b) symbol plane a) $a = 5$, b) $a = 1$, c) $a = 0.5$.

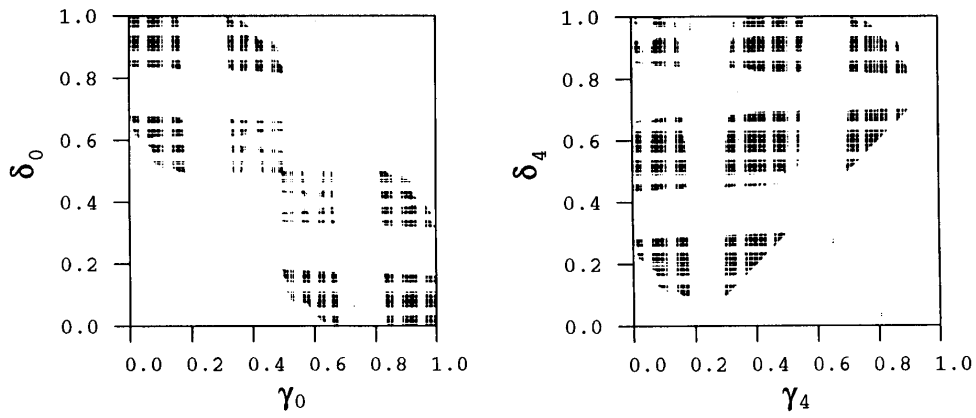


Figure 7.29: Bounces of a chaotic orbit in (γ^a, δ^a) for $a = 1$.

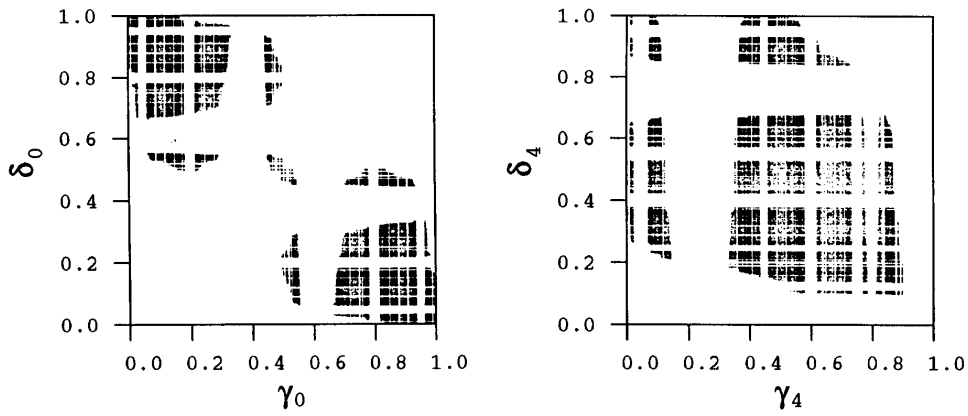


Figure 7.30: Bounces of a chaotic orbit in (γ^b, δ^b) for $a = 1$.

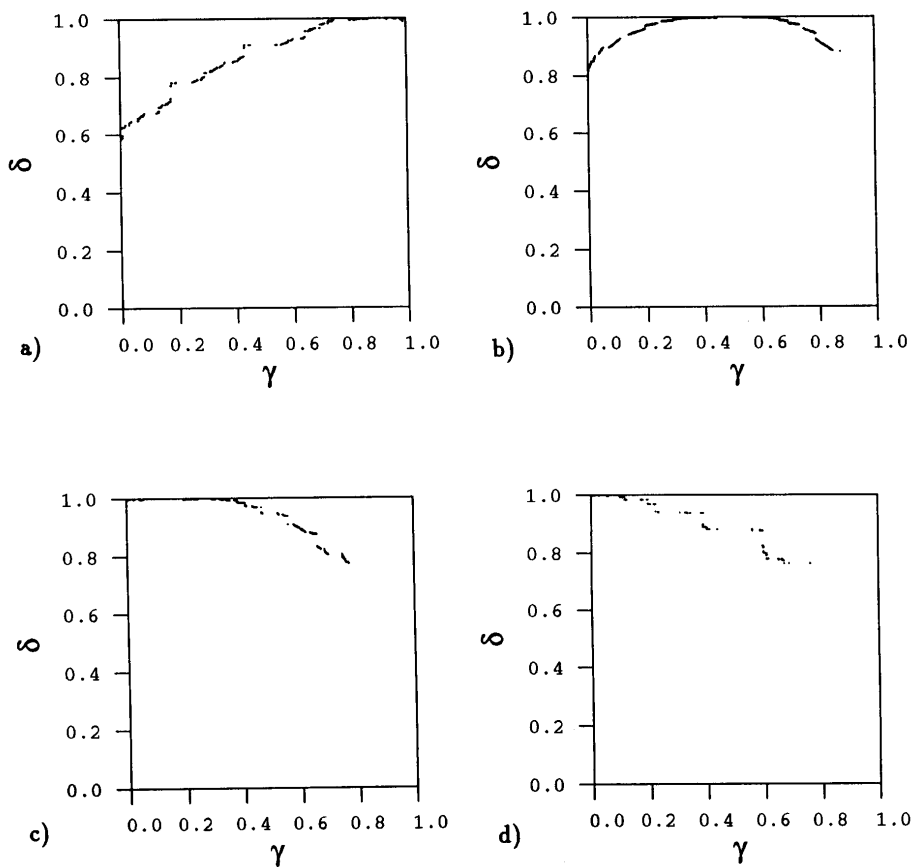


Figure 7.31: The pruning front for the wedge billiard. a) $\theta = 50^\circ$, b) $\theta = 60^\circ$, c) $\theta = 70^\circ$ and d) $\theta = 80^\circ$.

$w_{-1}^b w_0^b \cdot w_1^b w_2^b$	$s_t^b s_{t+1}^b \dots$
44 · 3	444455
34 · 3	244455
24 · 31	34445544
24 · 32	3444551
24 · 33	3444550
24 · 34	3444555
14 · 34	55444555
04 · 34	0444555
23 · 4	02442
3 · 42	24420
2 · 42	34420
41 · 42	2554420

a)

b)

Table 7.3: The parameter dependent completely pruned stings of length ≤ 4 for w^b for parameter $a = 1$. a) Symbols w_t^b . b) Some symbols s_t^b .

This corner is orbits having one symbol $s_t = 1$ with a long string of $s = 0$ symbols on each side of this symbol. A physical interpretation for the wedge billiard is that the orbits bouncing a number of times on one tilted wall then jumps over to the other tilted wall and bounces a number of times there are forbidden. This dynamics is difficult for the particle if the angle is close to $\theta = 45^\circ$ because then usually the particle will return immediately to the first wall giving a $s_t s_{t+1} = 11$ string. For the two ball system this dynamics is orbits where the down-most ball bounces a number of times off the floor, then bounces *once* into the uppermost ball and then continues to bounce off the floor a number of times. When the masses of the two balls are similar then this is an unlikely event because the balls tend to bounce twice. The dynamics for this limit is discussed further in section 8.1.

In the limit of $\theta = 90^\circ$ most of the forbidden orbits are orbits in the upper right corner. This corner gives the symbol strings where there is a symbol string $s_t s_{t+1} = 11$ surrounded by strings of symbol 0. In the wedge this is orbits crossing the tip twice which is difficult in the limit where the tip vanishes. In the two ball system this is a sequence of ball-ball; ball-floor; ball-ball collisions which is unlikely if the uppermost ball is much smaller than the downmost ball.

We find that the first region decreases and the second region increases as θ increases from $\theta = 45^\circ$ to $\theta = 90^\circ$. All parameters between $\theta = 45^\circ$ and $\theta = 90^\circ$

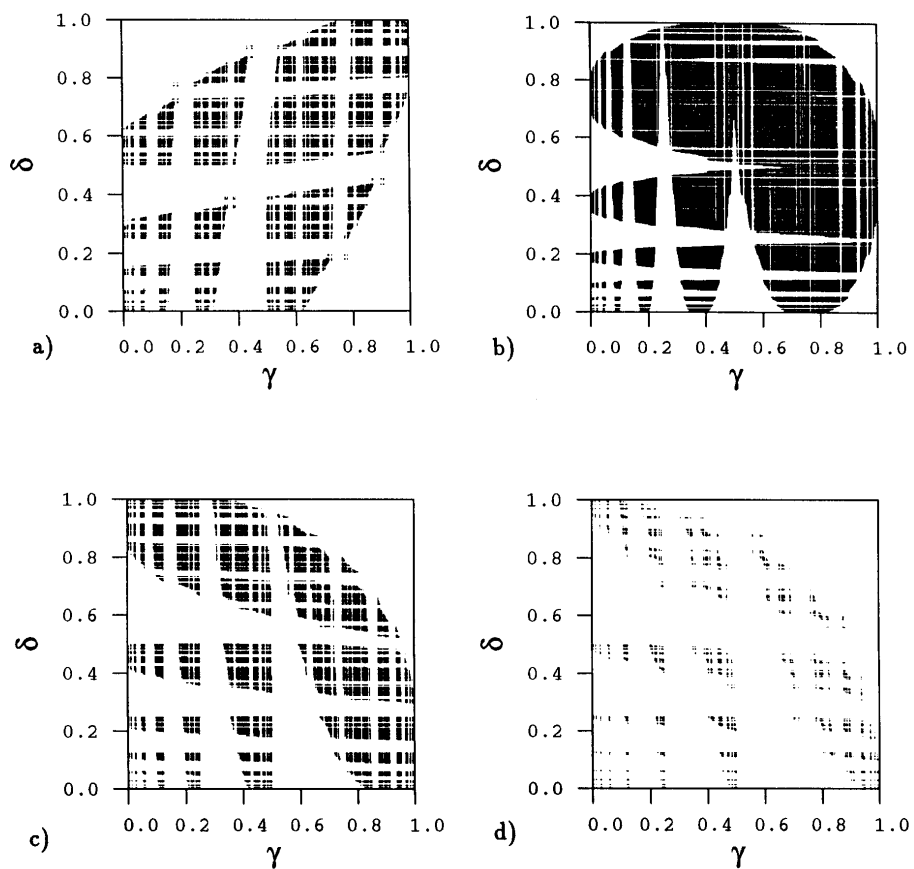


Figure 7.32: A chaotic orbit in the wedge billiard plotted in the symbol plane. a) $\theta = 50^\circ$, b) $\theta = 60^\circ$, c) $\theta = 70^\circ$ and d) $\theta = 80^\circ$.

$s_t s_{t+1} \dots$	
001100	000010011
0000110	110010000
0110000	011000110
0001000	001101100
00011011	0110011011
11011000	1101100110
00000100	1100110110
00100000	0110110011

Table 7.4: The forbidden strings up to length 10 of the wedge billiard; $\theta = 60^\circ$.

have a primary pruned region including both the upper left and the upper right corner.

As for the other systems we can approximate the pruning front by rectangles and get an approximate description of the admissible orbits for a given parameter value. For $\theta = 60^\circ$ we get the forbidden strings in table 7.4. Including strings up to length 10 gives the topological entropy $h = -\ln(0.522097\dots) = 0.64990\dots$. All the zeroes in the complex plane for this polynomeal is drawn in figure 7.33. The zeroes seems to build up a wall of convergence at the unit circle similar to the chaotic unimodal map in figure 1.24.

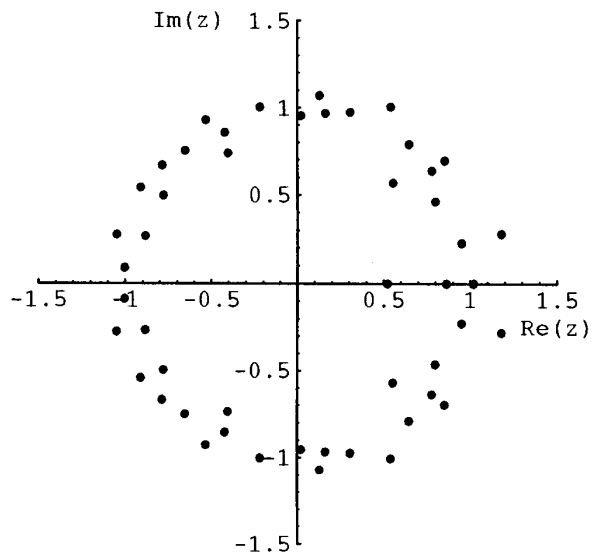


Figure 7.33: The zeroes of the characteristic polynomial for the wedge billiard; $\theta = 60^\circ$, with forbidden strings up to length 10.